Mechanical Behavior and Optimization of Functionally Graded Hollow Cylinder with an Elliptic Hole

J. Jafari Fesharaki [a,b*], M. Roghani[a,b]

[a] Department of Mechanical Engineering, Najafabad Branch, Islamic Azad University, Najafabad, Iran
[b] Modern Manufacturing Technologies Research center, Najafabad Branch, Islamic Azad University, Najafabad, Iran

A B S T R A C T

This paper presents a numerical solution and optimization for a functionally graded material cylinder with an elliptic hole subjected to mechanical pressure. To obtain the governing equations, an elliptic cylindrical coordinate was used. The material properties were considered in a way in order to vary with power-law function along the elliptic cylindrical direction. The differential quadrature method was used for solving the equations. In addition, by using von-Mises stress along with the thickness, the optimal values for various material inhomogeneity and the geometry of the cylinder investigated. The results showed that the inconsistency in shape of the hole in the cylindrical vessel can affect the expected results and the stresses in thickness of cylinder were changed. Furthermore, it was shown that with low values of the functionally graded material index, the geometry of the cylinder had a more significant effect on von Misses stress. Additionally, with high values for the material index, the values for von Misses stress converged together and the material inhomogeneity had a less noticeable effect on stress. The results also showed that for various geometries of the cylinder and holes, the best value for material homogeneity to reach the optimum value for von Misses stress was changed. The presented results were consistent with those reported in previous publications.

1. Introduction

Solving functionally graded material (FGM) problems mathematically is broadly utilized in numerous fields. FGM is in general a two-material composition in which the material properties vary continuously along certain directions and this variation presumes to be in exponential, power law or other functions along that desired direction. In addition, the Differential quadrature method (DQM) is an alternative to the conventional numerical methods for the solution of boundary and initial value problems. DQM offers more computational efficiency and numerical accuracy over its traditional competitors. For example, Ersoy et al. [1] studied about the frequencies of functionally graded annular plates and shells by DQM. They investigated the effects of different types of the grid distribution and grid number of shell and annular plates. In addition, Duc et al. [2] studied the vibration and nonlinear dynamic response of eccentrically stiffened the imperfect FGM elliptical cylinder subjected to the thermal field. Furthermore, by using complex Fourier series Fesharaki et al., obtained the exact solution for the electromechanical behavior of hollow cylinder made of functionally graded piezoelectric material [3, 4]. Bouhadra et al. [5] used higher order shear deformation theory for analysis of the composite plates. Alibeigloo [6] investigated the semi-analytical thermo-elasticity solution for a circular sandwich plate with FGM core. In another study, using the variational differential quadrature method, Ansari et al. [7] presented vibration analysis of spherical shells made of FGM carbon nanotube-reinforced composite resting on an elastic foundation. Also, using a double directors finite shell element, Frikha et al. [8] presented dynamic analysis of functionally graded CN-reinforced shell and plateuctures. The, theory of elasticity and DQM were used to analyze the free and the static vibration of cylindrical sandwich shells with FGM core layers by Alibeigloo and Noee [9].

Younsi et al. [10] presented a novel quasi 3-dimensional (3D) and 2-dimensional (2D) shear order deformation theory for analysis of bending and vibration of functionally graded material plates. Additionally, Nejati et al. [11] used the Von-Karman type strain-displacement and 3D elasticity theories to investigate the free vibration of rectangular plates with functionally graded fiber orientation under the effect of temperature. Fesharaki et al. [12, 13] studied the effect of stiffness ratio of patches and plates in to reduce the stress in a plate with a central hole. Furthermore, Fourn et al. [14] presented a novel refined plate theory for wave propagation in functionally graded material plates. Frikha et al. [15] also worked on analysis of functionally graded CN-reinforced composite shells with finite rotation with three and four node shell elements. Shojaee et al. [16] analyzed the behavior of functionally graded carbon nanotube-reinforced composite cylinders subjected to free vibration. They utilized Hamilton's principle to determine the governing differential equations and boundary conditions, and the first-order shear deformation shell theory was applied to model the deformation kinematics. Menasria et al. [17] presented a new higher order shear deformation theory for thermal stability analysis of functionally graded sandwich plates. Alibeigloo [18] obtained the thermo-elasticity solution of FGM solid annular and circular plates integrated with layers of piezoelectric material by using DQM. He investigated the effects of thickness to radius ratio, edge boundary conditions and the gradient index on the thermo-elastic behavior of functionally graded solid annular and circular plates. Zghal et al. [19] studied the static analysis of FG carbon nanotube-reinforced shell and plate structures. In another study, Atrian et al. [20] obtained an exact solution for thermo-electromechanical behavior of hollow cylinders made of functionally graded piezoelectric material under non-axisymmetric loads. Rashidifar et al. [21] worked on analysis of cylinders made of functionally graded piezoelectric material under thermal electro - mechanical loads. In further research by Hoshyarmanesh et al. [22] they investigated the composite piezo sensors used in aerospace structural health monitoring applications. Tornabene et al. [23] performed a numerical investigation by the local generalized differential quadrature method on the natural frequencies of functionally graded sandwich shells with variable thickness. Furthermore, Laplace transformation of time domain, state space technique along the radial direction and Fourier series expansions for displacements and stresses along the axial direction were used to work on a 3D transient analysis of functionally graded cylindrical shells subjected to mechanical and thermal loading by Ayoubi and Alibeigloo [24]. In addition, using the first order shear deformation theory, Trabelsi et al. [25, 26] studied the thermal post buckling analysis of functionally graded plates and cylindrical shells. Lei et al. [27] investigated vibration and thermal buckling of FGM sinusoidal microbeams using the differential quadrature method under nonlinear temperature distribution. Also, the Shooting method was used by Sun et al., to study the thermal post-buckling and buckling of functionally graded Timoshenko beams on a nonlinear elastic foundation [28]. Bakhadda et al. [29], worked on bending and dynamic analysis of carbon nanotube- reinforced composite plates with an elastic foundation. Fesharaki et al. [30] investigated the location of patches on plates to obtain maximum buckling load for a plate. Using finite e shell element, Zghal et al. [31-33] studied the free vibration and buckling analysis of functionally graded carbon nanotubes reinforced composite plates, shells and curved panels. Tornabene et al. [34] developed the boundary conditions in two and three-dimensional numerical models for analyzing cylindrical bending of FGM structures. They used the finite element and generalized differential quadrature methods and subsequently compared them with an exact 3D shell solution of free vibrations of FGM shells and plates. Using the von Karman nonlinear plate theory and the classical plate theory Kermani et al. performed a nonlinear stability analysis of transversal vibrations and rotational dynamics of FGM annular circular thin plates [35]. Abdelaziz et al. [36] investigated an efficient shear deformation theory for buckling, bending and free vibration of functionally graded material plates. Liew et al. [37] studied the nonlinear and linear vibration of a coating-FGM-substrate cylindrical panel under a temperature gradient. They showed that vibration amplitude had a significant influence on the nonlinear and linear vibration frequencies. Pradhan and Murmu [38] used the differential quadrature method to analyze the thermo-mechanical vibration of functionally graded sandwich beams resting on different elastic foundations. Based on the 2D theory of elasticity Chao-Feng and Chen presented the free vibration analysis of orthotropic FGM beams with different end conditions [39]. Vahdati et al. [40] worked on fracture analysis of piezo-electro-magnetic medium with axisymmetric cracks. Bellifa et al. [41] worked on buckling analysis of functionally graded plates using various refined plate theories. Yang et al. [42] investigated the thermo-mechanical post-buckling of functionally graded cylindrical panels considering temperature-

dependent properties. Also, using the differential quadrature method, Yas and Aragh [43] carried out the elasticity solution for analysis of free vibration of cylindrical panels with functionally graded fiber orientation.

The previous studies by Alle, focused on ideal cylinders but considering the fact that in many practical vessels, the inner radius of the cylinder is not exactly circular but almost non-circular shape, this inconsistency in the shape of a vessel can affect the values of the expected results. This behavior is very important, for example in sensor instruments. The novelty of this paper is that a cylinder with non-circular hole is investigated. For this purpose, a hollow cylinder with an elliptical hole, made of functionally graded material subjected to internal pressure was investigated. All governing equations extracted in the elliptic cylindrical were coordinated. The material properties were considered in order to vary along the elliptic cylindrical direction by a power function in ξ. To solve the problem, the differential quadrature method was used. The results for various values for the material gradient along the were cylinder presented. Then by considering von Misses stress, the optimum values of material inhomogeneity index and various geometries were investigated. Finally, results were compared with those reported in previous publications.

2. Problem definition

Consider a thick hollow cylinder made of functionally graded material with an elliptical hole. To solve the problem an elliptic cylindrical coordinate is considered. The considering problem and coordinate are shown in Fig. 1. For simplicity, the value a=1 is considered for elliptic cylinder located at the center of the cylinder.

According to non-uniform geometry (ellipse shape of the hole), the problem formulates in two directions. considering, "u" and "v" to be the displacements along the elliptic and hyperbolic cylindrical direction along "ξ" and "η" direction respectively. Thus, in the elliptic cylindrical coordinate system the relation between strains and displacements along the elliptic and hyperbolic cylindrical directions are (From appendix A1):

$$\varepsilon_{\xi\xi} = \frac{1}{A}\frac{\partial u}{\partial \xi} + \frac{\sin\eta \cdot \cos\eta}{A^3}v$$
$$\varepsilon_{\eta\eta} = \frac{1}{A}\frac{\partial v}{\partial \eta} + \frac{\sinh\eta \cdot \cosh\eta}{A^3}u$$
$$\varepsilon_{\xi\eta} = \frac{1}{2}\left(\frac{1}{A}\frac{\partial u}{\partial \eta} + \frac{1}{A}\frac{\partial v}{\partial \xi} - \frac{\sinh\xi \cdot \cosh\xi}{A^3}v \right. \tag{1}$$
$$\left. - \frac{\sin\eta \cdot \cos\eta}{A^3}u\right)$$

The relation between stress and strain in considering geometry can be presented as:

$$T_{\xi\xi} = N_{11}^F \cdot \varepsilon_{\xi\xi} + N_{12}^F \cdot \varepsilon_{\eta\eta} \tag{2}$$

$$T_{\eta\eta} = N_{12}^F \cdot \varepsilon_{\xi\xi} + N_{22}^F \cdot \varepsilon_{\eta\eta}$$
$$T_{\xi\eta} = 2N_{13}^F \cdot \varepsilon_{\xi\eta}$$

where T_{ij} $(i.j = \xi.\eta)$ and N_{ij}^F $(i.j = 1.2.3)$ are the stress tensor component and elastic coefficient respectively. The superscript "F" is used to show that the material properties are specified for functionally graded material. For calculating the functionally graded properties of material, suppose that all material coefficients are graded through the elliptic cylindrical direction "ξ", thus the material properties are functions of "ξ" as:

$$N_{ij}^F = N_{ij}\xi^p \qquad (i.j = 1.2.3) \tag{3}$$

Where the corresponding values of the outer surface of the cylinder show with N_{ij} and "p" is the power-law index of the functionally graded material properties.

The equilibrium equations for a functionally graded hollow cylinder in elliptical cylinder coordinate irrespective of inertia and body force along the hyperbolic and elliptic cylindrical directions respectively are expressed as (From appendix B).

$$\frac{\partial T_{\xi\xi}}{\partial \xi} + \frac{\partial T_{\xi\eta}}{\partial \eta} + \frac{2\sin\eta\cos\eta}{A^2}T_{\xi\eta}$$
$$+ \frac{\sinh\xi\cosh\xi}{A^2}(T_{\xi\xi} - T_{\eta\eta}) \tag{4}$$
$$= 0$$

$$\frac{\partial T_{\eta\eta}}{\partial \eta} + \frac{\partial T_{\xi\eta}}{\partial \xi} + \frac{2\sinh\xi\cosh\xi}{A^2}T_{\xi\eta}$$
$$+ \frac{\sin\eta\cos\eta}{A^2}(T_{\eta\eta} - T_{\xi\xi}) \tag{5}$$
$$= 0$$

Using equations (1) -(3) and substituting them into equations (4) and (5), the two coupled governing differential equations based on displacement components yields as:
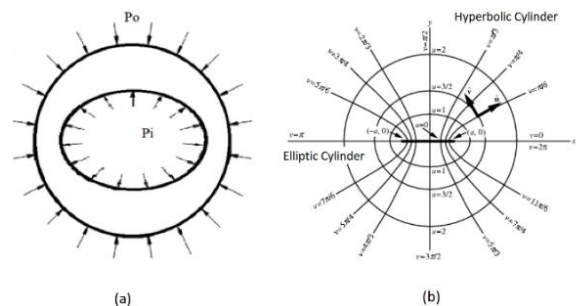

Fig. 1. (a) geometry model for considering the problem (b) considering coordinate (elliptic cylindrical)

$$\frac{\partial^2 u}{\partial \xi^2} + c_1 \frac{\partial^2 u}{\partial \eta^2} + \frac{p}{\xi} \frac{\partial u}{\partial \xi} + c_2 \frac{\sin \eta \cos \eta}{A^2} \frac{\partial u}{\partial \eta}$$

$$+ c_3 \frac{p}{\xi} \frac{\sinh \xi \cosh \xi}{A^2} u + c_4 \frac{\sinh^2 \xi \cosh^2 \xi}{A^4} u$$

$$+ c_3 \frac{\sinh^2 \xi}{A^2} u + c_3 \frac{\cosh^2 \xi}{A^2} u + c_8 \frac{\sin^2 \eta \cos^2 \eta}{A^4} u$$

$$+ c_9 \frac{\partial^2 v}{\partial \xi \partial \eta} + c_5 \frac{\sin \eta \cos \eta}{A^2} \frac{\partial v}{\partial \xi} \qquad (6)$$

$$+ c_6 \frac{\sinh \xi \cosh \xi}{A^2} \frac{\partial v}{\partial \eta} + c_3 \frac{p}{\xi} \frac{\partial v}{\partial \eta}$$

$$+ \frac{p}{\xi} \frac{\sin \eta \cos \eta}{A^2} v + c_7 \frac{\sin \eta \cos \eta \sinh \xi \cosh \xi}{A^4} v$$

$$= 0$$

$$\frac{\partial^2 v}{\partial \eta^2} + c_{10} \frac{\partial^2 v}{\partial \xi^2} + c_{11} \frac{\sin \eta \cos \eta}{A^2} \frac{\partial v}{\partial \xi} + c_{10} \frac{p}{\xi} \frac{\partial v}{\partial \xi}$$

$$+ c_{12} \frac{\sinh \xi \cosh \xi}{A^2} \frac{\partial v}{\partial \xi} + c_{13} \frac{\cos^2 \eta}{A^2} v + c_{14} \frac{v}{A^2}$$

$$+ c_{15} \frac{\sin^2 \eta \cos^2 \eta}{A^4} v + c_{12} \frac{\cosh^2 \xi}{A^2} v$$

$$+ c_{16} \frac{p}{\xi} \frac{\sinh \eta \cosh \eta}{A^2} v + c_{17} \frac{\sinh^2 \xi \cosh^2 \xi}{A^4} v$$

$$+ c_{18} \frac{\partial^2 u}{\partial \xi \partial \eta} + c_{19} \frac{\sin \eta \cos \eta}{A^2} \frac{\partial u}{\partial \xi} + c_{10} \frac{p}{\xi} \frac{\partial u}{\partial \xi} \qquad (7)$$

$$+ c_{20} \frac{\sinh \xi \cosh \xi}{A^2} \frac{\partial u}{\partial \eta}$$

$$+ c_{21} \frac{\sin \eta \cos \eta \sinh \xi \cosh \xi}{A^4} u$$

$$+ c_{10} \frac{p}{\xi} \frac{\sin \eta \cos \eta}{A^2} u = 0$$

Where the constant c_1 to c_{19} are presented in Appendix C. These two couple equations should be solved simultaneously to specify the displacements along two directions. Solving the governing differential equations (6) and (7), need boundary conditions from all possible boundary conditions that presented:

$$u(\xi.\eta) = u_0. \qquad v(\xi.\eta) = v_0.$$
$$T_{\xi\xi}(\xi.\eta) = T_{\xi\xi}^0. \qquad T_{\eta\eta}(\xi.\eta) = T_{\eta\eta}^0. \qquad (8)$$
$$T_{\xi\eta}(\xi.\eta) = T_{\xi\eta}^0.$$

Where, by substituting equation (1) into (2), the stress values in terms of displacements yield to:

$$T_{\xi\xi} = \frac{N_{11}}{A} \xi^p \frac{\partial u}{\partial \xi} + \frac{N_{11}}{A^3} \xi^p \sin \eta \cos \eta \, v$$
$$+ \frac{N_{12}}{A} \xi^p \frac{\partial v}{\partial \eta} \qquad (9)$$
$$+ \frac{N_{12}}{A^3} \xi^p \sinh \xi \cosh \xi \, u$$

$$T_{\eta\eta} = \frac{N_{12}}{A} \xi^p \frac{\partial u}{\partial \xi} + \frac{N_{12}}{A^3} \xi^p \sin \eta \cos \eta \, v$$
$$+ \frac{N_{22}}{A} \xi^p \frac{\partial v}{\partial \eta} \qquad (10)$$
$$+ \frac{N_{22}}{A^3} \xi^p \sinh \xi \cosh \xi \, u$$

$$T_{\xi\eta} = \frac{N_{13}}{A} \frac{\partial u}{\partial \eta} + \frac{N_{13}}{A} \frac{\partial v}{\partial \xi} - N_{13} \frac{\sinh \xi . \cosh \xi}{A^3} v$$
$$- N_{13} \frac{\sin \eta . \cos \eta}{A^3} u \qquad (11)$$

Furthermore, presenting analytical solutions for coupled differential equations (6) and (7) is very difficult and so a powerful numerical method (differential quadrature method-DQM) was used to solve the equations.

3. Solution by DQM

In order to find out the numerical results for solving equations (6) and (7), the differential quadrature (DQM) method is used. DQM is an efficient and simple technique to find the solution of nonlinear PDEs of boundary and initial problems. The basis of this method relies on approximating the derivatives of a function at any discrete point in a coordinate direction as the weighted summation of the function values in all the points in that direction. Thus, the DQM rule for nth order derivatives of a function, U(x), may be rewritten as:

$$\left. \frac{\partial^n U}{\partial x^n} \right|_{x=x_i} = \sum_{j=1}^{N} A_{ij}^{(n)} U(x_j) \quad i = 1.2. \dots. N \qquad (12)$$

Where N is the number of sample points in the x-direction and $A_{ij}^{(n)}$ are the weighting coefficients of the nth order derivative in the x-direction at the nth sample point.

The two most important steps in this method are: first determining the sufficient amount of sample points and their locations and second, calculating the weighting coefficients at each of these points. Previous research has shown that unequally spaced sampling points will cause results that were more accurate. For locating the sampling points in the hyperbolic cylindrical direction, we can use the Chebyshev-Gauss-Lobatto method, which gives the sampling points an unequal distance:

$$D_i = \frac{L}{2} \left(1 - \cos \frac{(i-1)\pi}{N-1} \right) \; ; \quad i = 1.2. \dots. N \qquad (13)$$

And for the elliptic cylindrical direction, equally spaced sampling points are used. Weighting coefficient values depend on the choice of the test function. In this problem, polynomial test functions are implemented for the elliptic cylindrical direction as:

$$U(\xi) = 1. \xi. \xi^2. \dots. \xi^{N-1} \qquad (14)$$

and to satisfy continuity in the elliptic cylindrical direction the harmonic trial functions [44] are taken as:

$$\begin{cases} U(\eta) = \cos[2(k-1)\pi\eta]; \\ \quad k = 1,2, \dots, \frac{N}{2} + 1 \\ U(\eta) = \sin\left[2\left(k - \frac{N}{2} - 1\right)\pi\eta\right]; \\ \quad k = \frac{N}{2} + 2, \frac{N}{2} + 3, \dots \end{cases} \qquad (15)$$

Substituting the test functions, equations (14) and (15) into equation (12) results in a system of equations, which by solving them may yield the weighting coefficients:

$$\sum_{j=1}^{N} (U_j) A_{ij}^{(n)} = \frac{\partial^n}{\partial x^n} U_j \Big|_{x=x_i} \quad ; \quad i.k = 1.2.\ldots N \quad (16)$$

After finding the first order weight coefficients $(A_{i.j})$, the second order weight coefficients $(B_{i.j})$ may easily be obtained as:

$$B_{i,j} = \sum_{k=1}^{N} A_{ik} A_{kj} \quad ; \quad (i.j = 1.2.\ldots N) \quad (17)$$

Using equations (12) to (17), the differential quadrature analog domain and boundary equations obtained are:

$$\sum_{j=1}^{N} B_{ij}^{\xi} U_i + c_1 \sum_{j=1}^{N} B_{ij}^{\eta} U_i + \frac{p}{\xi} \sum_{j=1}^{N} A_{ij}^{\xi} U_i$$
$$+ c_2 \frac{\sin \eta \cos \eta}{A^2} \frac{\partial u}{\partial \eta} + c_3 \frac{p}{\xi} \frac{\sinh \xi \cosh \xi}{A^2} u$$
$$+ c_4 \frac{\sinh^2 \xi \cosh^2 \xi}{A^4} u + c_3 \frac{\sinh^2 \xi}{A^2} u$$
$$+ c_3 \frac{\cosh^2 \xi}{A^2} u + c_8 \frac{\sin^2 \eta \cos^2 \eta}{A^4} u \quad (18)$$
$$+ c_9 \sum_{k=1}^{N} \sum_{j=1}^{N} A_{ij}^{\eta} A_{jk}^{\xi} V_i + c_5 \frac{\sin \eta \cos \eta}{A^2} \sum_{j=1}^{N} A_{ij}^{\xi} V_i$$
$$+ c_6 \frac{\sinh \xi \cosh \xi}{A^2} \sum_{j=1}^{N} A_{ij}^{\eta} V_i + c_3 \frac{p}{\xi} \sum_{j=1}^{N} A_{ij}^{\eta} V_i$$
$$+ \frac{p}{\xi} \frac{\sin \eta \cos \eta}{A^2} v + c_7 \frac{\sin \eta \cos \eta \sinh \xi \cosh \xi}{A^4} v$$
$$= 0$$

$$\sum_{j=1}^{N} B_{ij}^{\eta} V_i + c_{10} \sum_{j=1}^{N} B_{ij}^{\xi} V_i$$
$$+ c_{11} \frac{\sin \eta \cos \eta}{A^2} \sum_{j=1}^{N} A_{ij}^{\xi} V_i + c_{10} \frac{p}{\xi} \sum_{j=1}^{N} A_{ij}^{\xi} V_i$$
$$+ c_{12} \frac{\sinh \xi \cosh \xi}{A^2} \sum_{j=1}^{N} A_{ij}^{\xi} V_i + c_{13} \frac{\cos^2 \eta}{A^2} v$$
$$+ c_{14} \frac{v}{A^2} + c_{15} \frac{\sin^2 \eta \cos^2 \eta}{A^4} v + c_{12} \frac{\cosh^2 \xi}{A^2} v$$
$$+ c_{16} \frac{p}{\xi} \frac{\sinh \eta \cosh \eta}{A^2} v + c_{17} \frac{\sinh^2 \xi \cosh^2 \xi}{A^4} v \quad (19)$$
$$+ c_{18} \sum_{k=1}^{N} \sum_{j=1}^{N} A_{ij}^{\eta} A_{jk}^{\xi} U_i$$
$$+ c_{19} \frac{\sin \eta \cos \eta}{A^2} \sum_{j=1}^{N} A_{ij}^{\xi} U_i + c_{10} \frac{p}{\xi} \sum_{j=1}^{N} A_{ij}^{\xi} U_i$$
$$+ c_{20} \frac{\sinh \xi \cosh \xi}{A^2} \sum_{j=1}^{N} A_{ij}^{\eta} U_i$$
$$+ c_{21} \frac{\sin \eta \cos \eta \sinh \xi \cosh \xi}{A^4} u$$
$$+ c_{10} \frac{p}{\xi} \frac{\sin \eta \cos \eta}{A^2} u = 0$$

$$T_{\xi\xi} = \frac{N_{11}}{A} \xi^p \sum_{j=1}^{N} A_{ij}^{\xi} U_i + \frac{N_{11}}{A^3} \xi^p \sin \eta \cos \eta \, v$$
$$+ \frac{N_{12}}{A} \xi^p \sum_{j=1}^{N} A_{ij}^{\eta} V_i \quad (20)$$
$$+ \frac{N_{12}}{A^3} \xi^p \sinh \xi \cosh \xi \, u$$

$$T_{\eta\eta} = \frac{N_{12}}{A} \xi^p \sum_{j=1}^{N} A_{ij}^{\xi} U_i + \frac{N_{12}}{A^3} \xi^p \sin \eta \cos \eta \, v$$
$$+ \frac{N_{22}}{A} \xi^p \sum_{j=1}^{N} A_{ij}^{\eta} V_i \quad (21)$$
$$+ \frac{N_{22}}{A^3} \xi^p \sinh \xi \cosh \xi \, u$$

$$T_{\xi\eta} = \frac{N_{13}}{A} \sum_{j=1}^{N} A_{ij}^{\eta} U_i + \frac{N_{13}}{A} \sum_{j=1}^{N} A_{ij}^{\xi} V_i$$
$$- N_{13} \frac{\sinh \xi . \cosh \xi}{A^3} v \quad (22)$$
$$- N_{13} \frac{\sin \eta . \cos \eta}{A^3} u$$

where A_{ij}^{ξ} and A_{ij}^{η} are the first order weighting coefficients in ξ and η direction, B_{ij}^{ξ} and B_{ij}^{η} are the second order weighting coefficients in ξ and η direction respectively. These equations assemble a matrix equation of the form:

$$\begin{bmatrix} [S_{bb}] & [S_{bd}] \\ [S_{db}] & [S_{dd}] \end{bmatrix} \begin{Bmatrix} \Delta_b \\ \Delta_d \end{Bmatrix} = \begin{Bmatrix} f \\ 0 \end{Bmatrix} \quad (23)$$

where Δ_b and Δ_d are the vector of displacement components U, V, related to the boundary and domain grid points respectively. Using the static condensation method Eq. (23) then reduces to:

$$[-S_{db} S_{bb}^{-1} S_{bd} + S_{dd}]\{\Delta_d\} = \{0\} \quad (24)$$

Eq. (24) represents a standard eigenvalue problem and by solving it, the displacements of grid points are attained.

4. Results and discussions

4.1. Validation of the results

To validate the formulation and results, consider the points through the thickness of the cylinder on "x" axis which are located on direction $\eta = 0$. If assumed that $1.317 \le \xi \le 3.688$ and using equation (A1) and considering the hydrostatic pressure at the inner surface of the cylinder, the problem is similar to a cylinder with a circular hole with the inner and outer radius equal to $2 \le R \le 20$. By considering these conditions, the results compared with those reported in reference [45], for comparison purposes, two FGM indices p=0 and p=0.5 are considered. Fig. 2 shows the differences between the results presented in this paper and those reported in Fig. 3 of reference [45] and it can be seen that there is good agreement between the presented results and those reported in previous work.

4.2. Discussion

In order to solve the problem, consider a cylinder with inner radius $\xi = 1$ and outer radios $\xi = 2$. Considering the material properties at the inner radius according to equations (2) and (3) as:

$$N_{11} = 94e9 \ MPa, N_{12} = 40.4e9 \ MPa \\ N_{13} = 53.8e9 \ MPa, N_{22} = 94e9 \ MPa \tag{25}$$

Because the problem is symmetric with respect to both the X-axis and Y-axis, for simplicity the elliptic cylindrical boundary is solved for $0 \leq \eta \leq \pi/2$ (one-quarter of the considering geometry).

The outer boundary condition is clamped along ξ and η direction and there is hydrostatic pressure at the internal elliptic hole. The boundary conditions are considered as follows:

$$u(\xi.\eta) = v(\xi.\eta) = 0 \quad at \ \xi = 2 \\ T_{\xi\xi}(\xi.\eta) = 10^6 \ Pa \quad at \ \xi = 1 \\ T_{\eta\eta}(\xi.\eta) = 0. \quad at \ \xi = 1 \tag{26}$$
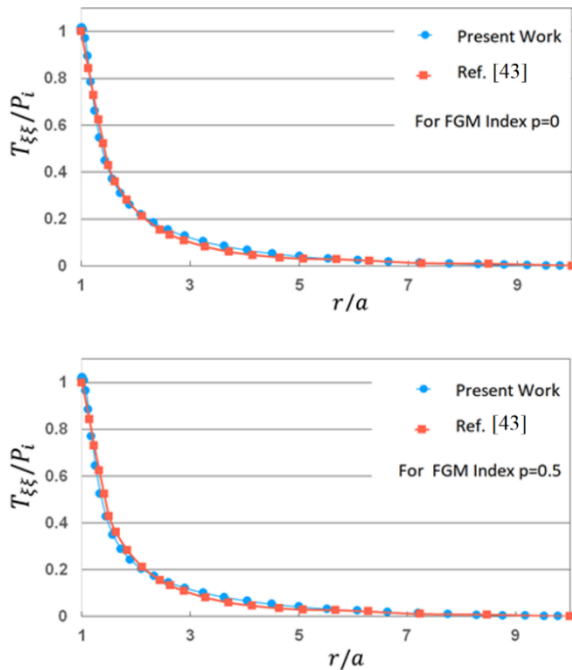
Fig. 2. Comparison of the Elliptic cylindrical stress with published literature for two power law index (p=0; p=0.5)
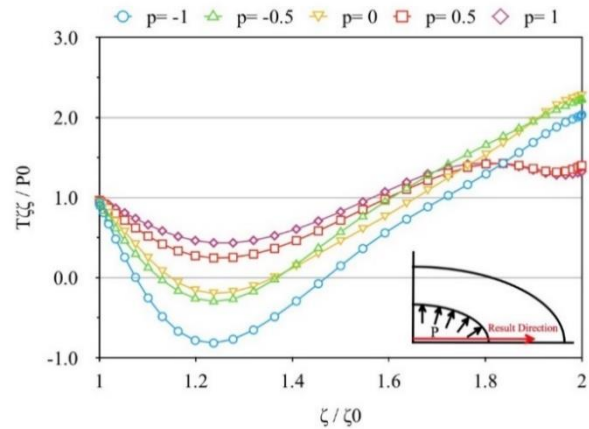

Fig. 3. Elliptic cylindrical stress for the various material index at $\eta = 0$
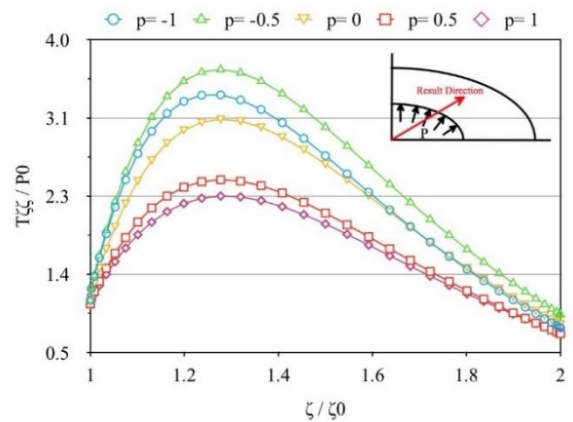

Fig. 4. Elliptic cylindrical stress for the various material index at $\eta = \frac{\pi}{4}$

Figures 3, 4 and 5 show the elliptic cylindrical stress for various material inhomogeneities along a line in a specified direction namely, $\eta = 0, \pi/4, \pi/2$ respectively. It can be seen from Fig. 3 that the values for elliptic cylindrical stress initially decrease from inside of the vessel and then increase to the outside of the vessel. In addition, this behaviour is the same for all material inhomogeneity indices. But by decreasing the material inhomogeneity, the intensity of decreasing/increasing the stress will be affected. Also, for material inhomogeneity near p=1, the changes in stress values are less than other values for material inhomogeneity. It should be noted that for material inhomogeneity near p=1, the elliptic cylindrical stress has almost two relative minimum values and this is because of the shape of the geometry, considering that it is different from the real cylinder. Fig. 4 shows the elliptic cylindrical stress at direction $\eta = \pi/4$. It can be seen that the values of stresses have the same manner for every material inhomogeneity but the index p=0 has a minimum value between all material inhomogeneities. Fig. 5 shows the results for elliptic cylindrical stress along $\eta = \pi/2$. The behavior is almost similar to those

reported in Fig. 3, along $\eta = 0$. By comparing the three Figs. 3, 4 and 5 together, the behaviour of elliptic cylindrical stress along the hyperbolic cylindrical direction is declared.

Figures 6, 7 and 8 show the hyperbolic cylindrical stress for various material inhomogeneities along a line in a specified direction $\eta = 0, \pi/4,\ \pi/2$ respectively. It can be seen that in directions $\eta = 0, \pi/2$ the values of hyperbolic cylindrical stress increases from the inside of the vessel to the near middle of the vessel and then it decreases in values for the outer of the vessel.

But for direction $\eta = \pi/4$ the values of stress have reverse behaviours. As mentioned before, these behaviours occur because of the asymmetry in the considered geometry. In addition, it can be seen that the material inhomogeneity near $p = 1$ produces minimum values in stress along the cylinder. It should be mentioned that the maximum value for stress occurs between $0 < \eta < \frac{\pi}{2}$.
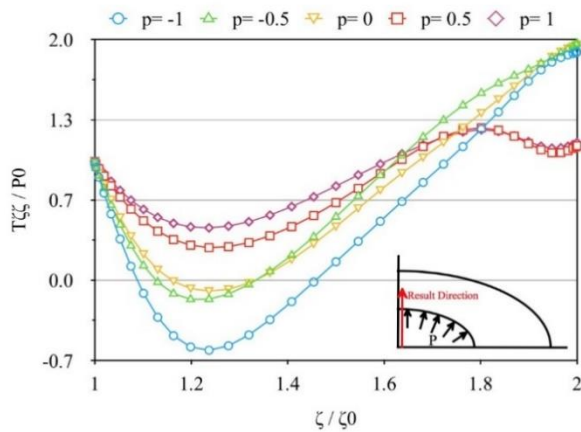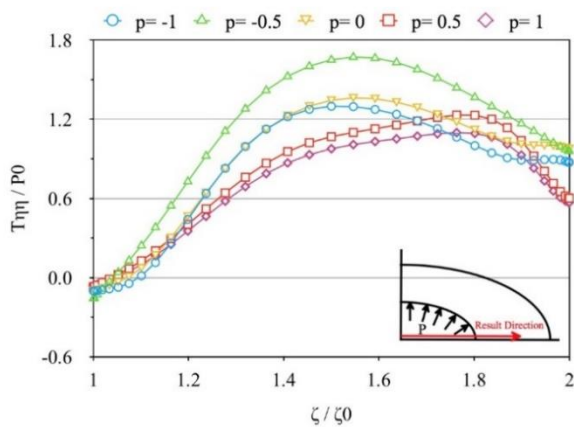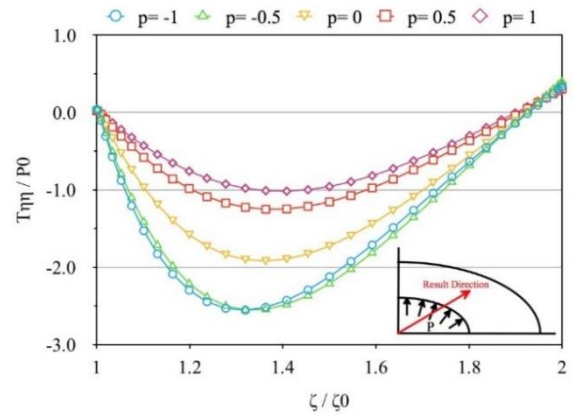

Fig. 7. Hyperbolic cylindrical stress for the various material index at $\eta = \frac{\pi}{4}$

Fig. 8. Hyperbolic cylindrical stress for the various material index at $\eta = \frac{\pi}{2}$
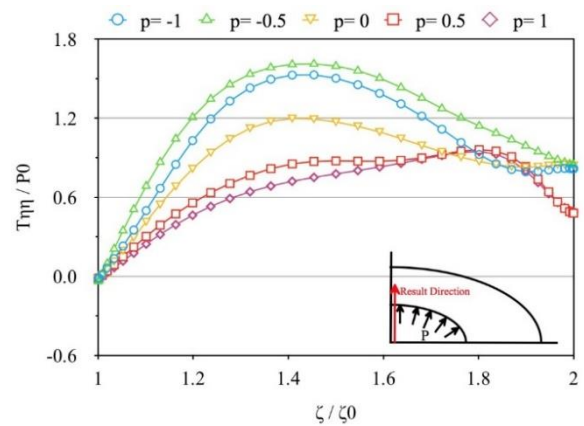

Fig. 5. Elliptic cylindrical stress for the various material index at $\eta = \frac{\pi}{2}$

Figures 9, 10 and 11 show the shear stress ($T_{\xi\eta}$) for various material inhomogeneity along three considering direction $\eta = 0, \pi/4,\ \pi/2$ respectively. It can be seen that at $\eta = 0$, the shear stress has more changes in value from inside to outside of the thickness of the vessel and these intensities decrease along the $\eta = \pi/4$ and $\eta = \pi/2$. Fig. 11 shows that the shear stress at $\eta = \pi/2$ almost has no changes from inner to outer of the vessel and only the material inhomogeneity affects the value of shear stress in the vessel. In addition, it can be seen from Figs. 9 to 11 that the slope of shear stress curves at the inner radius has higher values and near the outer of the vessel the shear stress has no changes.
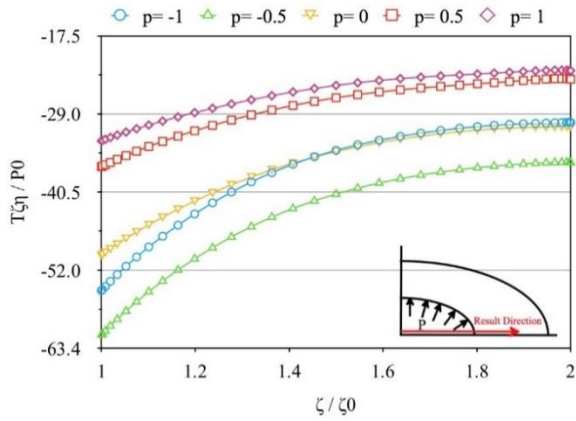

Fig. 6. Hyperbolic cylindrical stress for the various material index at $\eta = 0$

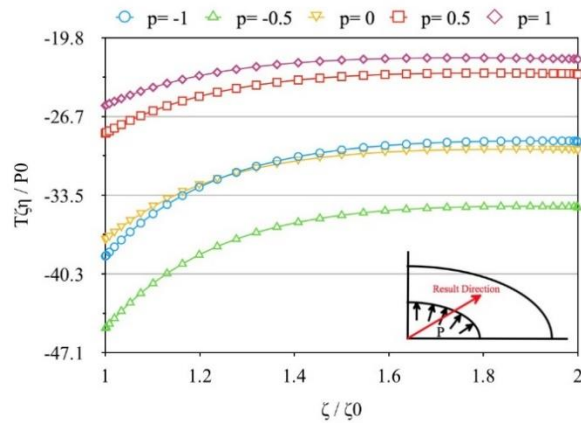**Fig. 9.** Shear stress for the various material index at $\eta = 0$

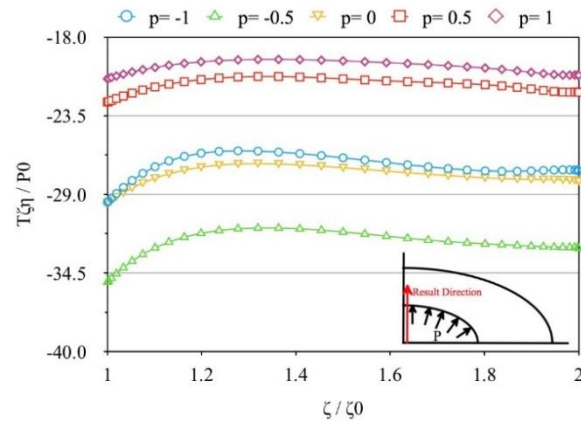**Fig. 10.** Shear stress for the various material index at $\eta = \frac{\pi}{4}$

Fig. 11. Shear stress for the various material index at $\eta = \frac{\pi}{2}$

The 3D stresses along the thickness of the cylinder for FGM index p=0.5 (for example) are shown in Figs. 12 to 14. Fig. 12 shows the elliptical cylindrical stress through the one-quarter of the cylinder for p=0.5. It can be seen that the considering boundary conditions in equation (26) are satisfied. In addition, the stress in the middle of the cylinder has maximum value and it changes along elliptical cylindrical and hyperbolic cylindrical direction. Figs. 13 and 15 show the hyperbolic cylindrical and shear stresses respectively. It can be seen from Fig. 14

that, because of the asymmetric geometry of the cylinder, the shear stress increases along the two considering directions for the problem. Also, it can be noted from Figs. 12 to 14 that, in this research, similar to the stress of considering the geometry, the shear stress will be very significant.

Figures 15 and 16 presented the elliptic cylindrical and hyperbolic cylindrical displacements through the thickness of the cylinder. It can be seen that according to considering boundary conditions in the outer surface of the cylinder, the displacements lead to zero value. Also, on the inner surface of the cylinder, the elliptic cylindrical displacement has a variable value, but the hyperbolic cylindrical displacement has a constant value and the changes through the hyperbolic cylindrical direction are negligible.
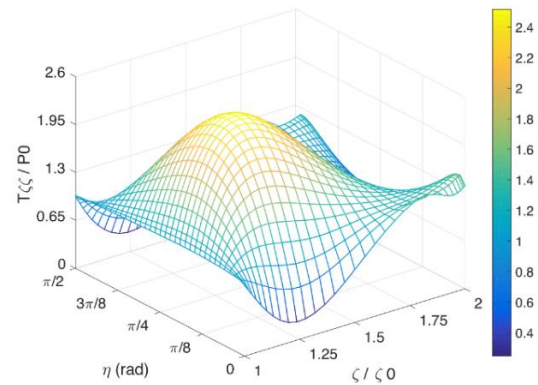

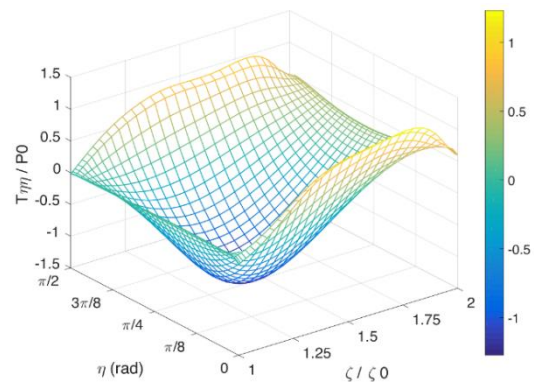**Fig. 12.** Elliptic cylindrical stress in the FGM cylinder with an elliptical hole for p=0.5

Fig. 13. Hyperbolic cylindrical stress in the FGM cylinder with an elliptical hole for p=0.5
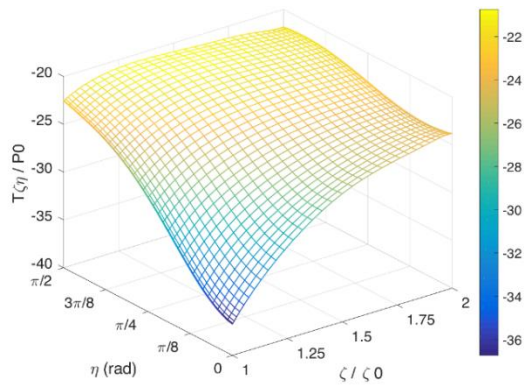
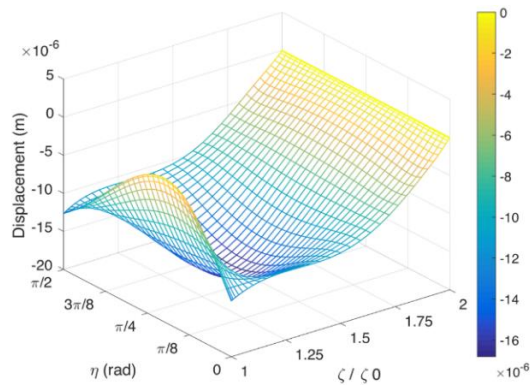**Fig. 14.** Shear stress in the FGM cylinder with an elliptical hole for p=0.5

Fig. 15. Elliptic cylindrical displacement in the FGM cylinder with an elliptical hole for p=0.5
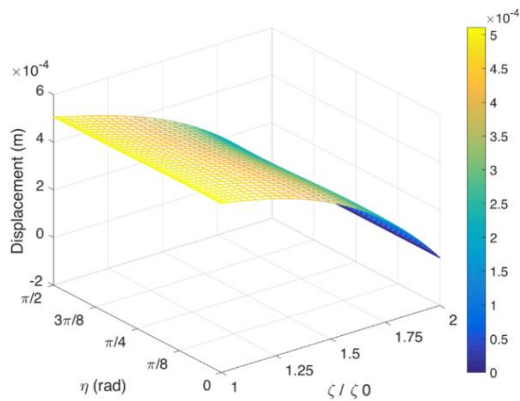

Fig. 16. Hyperbolic cylindrical displacement in the FGM cylinder with an elliptical hole for p=0.5

5. Aspect ratio effect

One of the most important issues about functionally graded material is that the material inhomogeneity index, leads to minimal stress in geometry. Also, the aspect ratio (ξ_o/ξ_i) of the cylinder, affects the stress in the cylinder. To investigate the aspect ratio of the cylinder and material inhomogeneity on stress in thickness of the cylinder, the von-Mises stress in the cylinder is considered. The von-Mises stress in plane stress condition is expressed as:

$$T_{von} = (T_{\xi\xi}^2 + T_{\eta\eta}^2 - T_{\xi\xi}T_{\eta\eta} + 3T_{\xi\eta}^2)^{1/2} \qquad (27)$$

By considering various material inhomogeneity as "P" and using the above method, the effects of the material index and ξ_o/ξ_i is presented in Fig. 17. It can be seen that the material inhomogeneity has much effect on von Misses stress and for each ratio ξ_o/ξ_i, at a specific material inhomogeneity index, the curves have an absolute minimum point. But the location of the minimum point is changed by any ratio ξ_o/ξ_i. For ratio $\xi_o/\xi = 2$, the minimum von Misses stress occurs near the material inhomogeneity index $p = 0$. But by increasing the ratio ξ_o/ξ_i, the optimum location for "p" is increased. For ratio $\xi_o/\xi = 5$, the optimum location occurs at about $p = 1.9$ for material inhomogeneity.

Another point of view is that by increasing the material inhomogeneity more than 4, the values for von Misses stress converge together. So, it can be concluded that if by increasing the material inhomogeneity high enough, the ratio ξ_o/ξ_i has the same effect on von Misses stress and by considering low values for the material inhomogeneity, the ratio ξ_o/ξ_i has more influence on von Misses stress.

6. Conclusions

This paper presents a numerical solution for a functionally graded material cylinder with an elliptic hole. Because of the difficulty in solving the considered geometry, the elliptic cylindrical coordinate is used for the governing equation and boundary condition. The material properties are varied along the elliptic cylindrical direction with power-law function. Because of the asymmetry in geometry, the equilibrium equations presented in elliptic cylindrical and hyperbolic cylindrical directions, for solving two coupled governing equation, the differential quadrature method is used. The results show that the existence of an elliptic hole in the cylinder changes the stress in the thickness of cylinder, effectively. Then, by computing von Misses stress along the thickness, the optimal values for various material inhomogeneities and various values for ξ_o/ξ_i is investigated. The results show that with low values for the material inhomogeneity index, the ratio ξ_o/ξ_i has more effect on von Misses stress. Also, with high values of the material index, the values for von Misses stress converge together and the material inhomogeneity has less effect on von Misses stress. Also, the results show that by increasing the ratio ξ_o/ξ_i, the optimum value of von Misses stress occurs at high-value material inhomogeneity index. The results presented in this paper are compared with those reported in previous work.
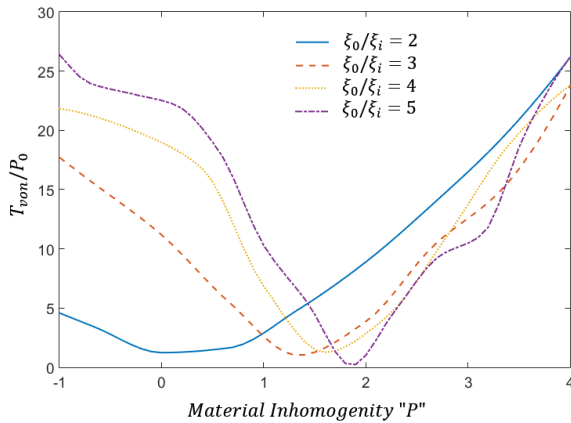
Fig. 17. effect of material inhomogeneity and ξ_o/ξ_i on von-Misses stress

Appendix A

The relations between Cartesian and Elliptic cylindrical coordinate are presented as [46]:

$$x = \cosh\xi\cos\eta \quad \xi \geq 0.$$
$$h_1 = \sqrt{\sinh^2\xi + \sin^2\eta}$$
$$y = \sinh\xi\sin\eta . 0 \leq \eta \leq 2\pi. \quad \text{(A1)}$$
$$h_2 = \sqrt{\sinh^2\xi + \sin^2\eta}$$
$$z = z. \quad \infty < z < \infty \quad h_3 = 1$$

And the coordinate curves formed by the intersection of coordinate:

For Elliptic Cylinders:
$$\frac{x^2}{\cosh^2\xi} + \frac{y^2}{\sinh^2\xi} = 1$$

For Hyperbolic Cylinders: (A2)
$$\frac{x^2}{\cos^2\eta} - \frac{y^2}{\sin^2\eta} = 1$$

$$z = Constant$$

So, the position vector for each point is:

$$\vec{r} = (\cosh\xi . \cos\eta)\vec{\imath} + (\sinh\xi . \sin\eta)\vec{\jmath} + z\vec{k} \quad \text{(A3)}$$

And the unit vector for each direction is presented as:

$$\hat{e}_\xi = \frac{1}{h_1}e_\xi = \frac{\sinh\xi . \cos\eta}{A}\vec{\imath} + \frac{\cosh\xi . \sin\eta}{A}\vec{\jmath}$$
$$\hat{e}_\eta = \frac{1}{h_2}e_\eta = \frac{-\cosh\xi . \sin\eta}{A}\vec{\imath} + \frac{\sinh\xi . \cos\eta}{A}\vec{\jmath} \quad \text{(A4)}$$
$$\hat{e}_z = \frac{1}{h_3}e_z = \vec{k}$$

Which, "A" for simplicity is defined as:

$$A = \sqrt{\sinh^2\xi + \sin^2\eta} \quad \text{(A5)}$$

Considering the displacement vector in elliptic cylindrical coordinate as:

$$\vec{u} = u\hat{e}_\xi + v\hat{e}_\eta + w\hat{e}_z \quad \text{(A6)}$$

The strain tensor is presented as:

$$\varepsilon = \frac{1}{2}(\nabla u + \nabla u^T) \quad \text{(A7)}$$

Substituting equation (A6) to (A7) and using equations (A1) to (A5) the strains yield as:

$$\varepsilon_{\xi\xi} = \frac{1}{A}\frac{\partial u}{\partial \xi} + \frac{\sin\eta . \cos\eta}{A^3}v$$
$$\varepsilon_{\eta\eta} = \frac{1}{A}\frac{\partial v}{\partial \eta} + \frac{\sinh\eta . \cosh\eta}{A^3}u$$
$$\varepsilon_{\xi\eta} = \frac{1}{2}\left(\frac{1}{A}\frac{\partial u}{\partial \eta} + \frac{1}{A}\frac{\partial v}{\partial \xi} - \frac{\sinh\xi . \cosh\xi}{A^3}v \right. \quad \text{(A8)}$$
$$\left. - \frac{\sin\eta . \cos\eta}{A^3}u\right)$$

Appendix B

Considering the static equilibrium equation in a linear elastic material expressed as:

$$T^i_{i.j} + \varrho b_i = 0 \quad i.j = 1.2.3 \quad \text{(B1)}$$

Where $T^i_{i.j}$ are the component of the stress tensor, ϱ is the density and b_i is the external body forces per unit mass of the material. By Assuming an orthogonal coordinate system, the $T^i_{i.j}$ is expressed as [46]:

$$T^i_{i.j} = \frac{1}{\sqrt{g}}\frac{\partial}{\partial x^j}\left(\sqrt{g}T^j_i\right) - [ij.m]T^{mj} \quad \text{(B2)}$$

Where "g" is the metric components of the orthogonal system and can be expressed as:

$$g_{ij} = \begin{pmatrix} h_1^2 & 0 & 0 \\ 0 & h_2^2 & 0 \\ 0 & 0 & h_3^2 \end{pmatrix} \quad \text{(B3)}$$

And in terms of physical components, the equilibrium equations are presented as:

$$\sum_{j=1}^{3}\frac{1}{\sqrt{g}}\frac{\partial}{\partial x^j}\left(\frac{\sqrt{g}h_i T_{ij}}{h_j}\right) - \frac{1}{2}\sum_{j=1}^{3}\frac{T_{jj}}{h_j^2}\frac{\partial(h_j^2)}{\partial x^i} + h_i\varrho b_i \quad \text{(B4)}$$
$$= 0$$

Where there is no summation on "i". So, the equilibrium equations in for two directional problems are expressed:

$$\frac{\partial T_{\xi\xi}}{\partial \xi} + \frac{\partial T_{\xi\eta}}{\partial \eta} + \frac{2\sin\eta\cos\eta}{A^2}T_{\xi\eta}$$
$$+ \frac{\sinh\xi\cosh\xi}{A^2}(T_{\xi\xi} - T_{\eta\eta})$$
$$= 0$$
$$\frac{\partial T_{\eta\eta}}{\partial \eta} + \frac{\partial T_{\xi\eta}}{\partial \xi} + \frac{2\sinh\xi\cosh\xi}{A^2}T_{\xi\eta} \quad \text{(B5)}$$
$$+ \frac{\sin\eta\cos\eta}{A^2}(T_{\eta\eta} - T_{\xi\xi})$$
$$= 0$$

Appendix C

The constants for material properties for equations (6) and (7):

$$c_1 = \frac{N_{13}}{N_{11}}. \quad c_2 = \frac{2N_{13}}{N_{11}}. \quad c_3 = \frac{N_{12}}{N_{11}}.$$
$$c_4 = \frac{-2N_{12} - N_{22}}{N_{11}}. \quad c_5 = \frac{N_{13} + N_{11}}{N_{11}}.$$
$$c_6 = \frac{-N_{13} - N_{22}}{N_{11}}. \quad c_7 = \frac{-N_{13} - 2N_{11} - N_{12}}{N_{11}}. \quad \text{(C1)}$$
$$c_8 = \frac{-N_{13}}{N_{11}}. \quad c_9 = \frac{N_{13} + N_{12}}{N_{11}}. \quad c_{10} = \frac{N_{13}}{N_{22}}.$$

$$c_{11} = \frac{N_{12} - N_{22}}{N_{22}}. \quad c_{12} = \frac{-2N_{13}}{N_{22}}.$$

$$c_{13} = \frac{2N_{12}}{N_{22}}. \quad c_{14} = \frac{-N_{12} - N_{13}}{N_{22}}.$$

$$c_{15} = \frac{-2N_{12} - N_{11}}{N_{22}}. \quad c_{16} = \frac{-N_{13}}{N_{22}}.$$

$$c_{17} = \frac{3N_{13}}{N_{22}}. \quad c_{18} = \frac{2N_{12} + N_{13}}{N_{22}}.$$

$$c_{19} = \frac{N_{13} - N_{11}}{N_{22}}. \quad c_{20} = \frac{N_{22} - N_{13}}{N_{22}}.$$

$$c_{21} = \frac{-2N_{22} - 3N_{13} - N_{12}}{N_{22}}$$

References

[1] Ersoy, H., Mercan, K. and Civalek, Ö., 2018. Frequencies of FGM shells and annular plates by the methods of discrete singular convolution and differential quadrature methods. Composite Structures, 183 (Supplement C), pp.7-20.

[2] Dinh Duc, N., Dinh Nguyen, P. and Dinh Khoa, N., 2017. Nonlinear dynamic analysis and vibration of eccentrically stiffened S-FGM elliptical cylindrical shells surrounded on elastic foundations in thermal environments. Thin-Walled Structures, 117 (Supplement C), pp.178-189.

[3] Jafari Fesharaki, J., Jafari Fesharaki, V., Yazdipoor, M. and Razavian, B., 2012. Two-dimensional solution for electro-mechanical behavior of functionally graded piezoelectric hollow cylinder. Applied Mathematical Modelling, 36(11), pp.5521-5533.

[4] Fesharaki, J.J. and Roghani, M., 2019. Thermo-mechanical behavior of a functionally graded hollow cylinder with an elliptic hole. Journal of the Brazilian Society of Mechanical Sciences and Engineering, 42(1), pp. 66.

[5] Abdelhakim, B., Tounsi, A., Bousahla, A., Benyoucef, S. and Mahmoud, SR, 2018. Improved HSDT accounting for effect of thickness stretching in advanced composite plates. Structural Engineering and Mechanics, 66(1), pp.61-73.

[6] Alibeigloo, A., 2016. Thermo elasticity solution of sandwich circular plate with functionally graded core using generalized differential quadrature method. Composite Structures, 136(Supplement C), pp.229-240.

[7] Ansari, R., Torabi, J. and Shojaei, M.F., 2016. Vibrational analysis of functionally graded carbon nanotube-reinforced composite spherical shells resting on elastic foundation using the variational differential quadrature method. European Journal of Mechanics-A/Solids, 60(Supplement C), pp.166-182.

[8] Frikha, A., Zghal, S. and Dammak, F., 2018. Dynamic analysis of functionally graded carbon nanotubes-reinforced plate and shell structures using a double directors finite shell element. Aerospace Science and Technology, 78, pp.438-451.

[9] Alibeigloo, A. and Rajaee, A., 2017. Static and free vibration analysis of sandwich cylindrical shell based on theory of elasticity and using DQM. Acta Mechanica, 228(12), pp.4123-4140.

[10] Younsi, A., Tounsi, A., Zaoui, F.Z., Bousahla, A.A. and Mahmoud, S.R., 2018. Novel quasi-3D and 2D shear deformation theories for bending and free vibration analysis of FGM plates. Geomechanics and Engineering, 14(6), pp.519-532.

[11] Nejati, M., Yas, M.H., Eslampanah, A. and Bagheriasl, M., 2017. Extended three-dimensional generalized differential quadrature method: The basic equations and thermal vibration analysis of functionally graded fiber orientation rectangular plates. Mechanics of Advanced Materials and Structures, 24(10), pp.854-870.

[12] Fesharaki, J.J. and Golabi, S. 2017, Effect of stiffness ratio of piezoelectric patches and plate on stress concentration reduction in a plate with a hole. Mechanics of Advanced Materials and Structures, 24(3), pp.253-259.

[13] Fesharaki, J.J., Madani, S.G. and Golabi, S., 2016, Effect of stiffness and thickness ratio of host plate and piezoelectric patches on reduction of the stress concentration factor. International Journal of Advanced Structural Engineering, 8(3), pp.229-242.

[14] Fourn, H., Atmane, H.A., Bourada, M., Bousahla, A.A., Tounsi, A. and Mahmoud, S.R., 2018, A novel four variable refined plate theory for wave propagation in functionally graded material plates. Steel and Composite Structures, 27(1), pp.109-122.

[15] Frikha, A., Zghal, S. and Dammak, F., 2018, Finite rotation three and four nodes shell elements for functionally graded carbon nanotubes-reinforced thin composite shells analysis. Computer Methods in Applied Mechanics and Engineering, 329, pp.289-311.

[16] Shojaee, M., Setoodeh, A.R. and Malekzadeh, P., 2017, Vibration of functionally graded CNTs-reinforced skewed cylindrical panels using a transformed differential quadrature method. Acta Mechanica, 228(7), pp.2691-2711.

[17] Menasria, A., Bouhadra, A., Tounsi, A. and Bousahla, A.A., 2017, A new and simple HSDT for thermal stability analysis of FG sandwich plates. Steel and Composite Structures, 25(2), pp.157-175.

[18] Alibeigloo, A., 2017, Thermo elasticity solution of functionally graded, solid, circular, and annular plates integrated with piezoelectric layers using the differential quadrature method. Mechanics of Advanced Materials and Structures, pp. 1-19.

[19] Zghal, S., Frikha, A. and Dammak, F., 2017, Static analysis of functionally graded carbon nanotube-reinforced plate and shell structures. Composite Structures, 176, pp.1107-1123.

[20] Atrian, A., Jafari Fesharaki, J. and Nourbakhsh, S.H., 2015, Thermo-electromechanical behavior of functionally graded piezoelectric hollow cylinder under non-axisymmetric loads. Applied Mathematics and Mechanics, 36(7), pp.939-954.

[21] Rashidifar, R., Jafari, J., Shahriary, H. and Jafari, V., 2014, Analysis of FGPM cylinder subjected to two dimensional electro thermo mechanical fields. Modares Mechanical Engineering, 14(4), pp.83-90.

[22] Hoshyarmanesh, H., Ebrahimi, N., Jafari, A., Hoshyarmanesh, P., Kim, M., Park, H.H., 2018, PZT/PZT and PZT/BiT Composite Piezo-Sensors in Aerospace SHM Applications: Photochemical Metal Organic+Infiltration Deposition and Characterization. Sensors, 19(1), pp.13.

[23] Tornabene, F., Fantuzzi, N., Bacciocchi, M., Viola, E. and Reddy, J. N., 2017, A Numerical Investigation on the Natural Frequencies of FGM Sandwich Shells with Variable Thickness by the Local Generalized Differential Quadrature Method, Applied Sciences, 7(2), pp.131.

[24] Ayoubi, P. and Alibeigloo, A., 2017, Three-dimensional transient analysis of FGM cylindrical shell subjected to thermal and mechanical loading. Journal of Thermal Stresses, 40(9), pp.1166-1183.

[25] Trabelsi, S., Frikha, A., Zghal, S. and Dammak, F., 2019, A modified FSDT-based four nodes finite shell element for thermal buckling analysis of functionally graded plates and cylindrical shells. Engineering Structures, 178, pp.444-459.

[26] Trabelsi, S., Frikha, A., Zghal, S. and Dammak, F., 2018, Thermal post-buckling analysis of functionally graded material structures using a modified FSDT, International Journal of Mechanical Sciences, 144, pp. 74-89.

[27] Lei, J., He, Y., Guo, S. and Zhenkun, L., 2017, Thermal buckling and vibration of functionally graded sinusoidal microbeams incorporating nonlinear temperature distribution using DQM. Journal of Thermal Stresses, 40(6), pp.665-689.

[28] Sun, Y., Li, S.R. and Batra, R.C., 2016, Thermal buckling and post-buckling of FGM Timoshenko beams on nonlinear elastic foundation, Journal of Thermal Stresses, 39(1), pp.11-26.

[29] Bakhadda, B., Bouiadjra, M.B., Bourada, F., Bousahla, A.A., Tounsi, A. and Mahmoud, S.R., 2018, Dynamic and bending analysis of carbon nanotube-reinforced composite plates with elastic foundation. Wind and Structures, 27(5), pp.311-324.

[30] Jafari Fesharaki, J., Dehkordi, H.M., Zohari, M. and Karimi, S., 2018, Best pattern for locating piezoelectric patches on a plate for maximum critical buckling loads, using particle swarm optimization algorithm. Journal of Intelligent Material Systems and Structures, 29(14), pp.2874-2884.

[31] Zghal, S., Frikha, A. Dammak, F., 2018, Free vibration analysis of carbon nanotube-reinforced functionally graded composite shell structures. Applied Mathematical Modelling, 53, pp.132-155.

[32] Zghal, S., Frikha, A. and Dammak, F., 2018, Mechanical buckling analysis of functionally graded power-based and carbon nanotubes-reinforced composite plates and curved panels. Composites Part B: Engineering, 150, pp. 165-183.

[33] Zghal, S., Frikha, A., Dammak, F., 2018, Non-linear bending analysis of nanocomposites reinforced by graphene-nanotubes with finite shell element and membrane enhancement. Engineering Structures, 158, pp.95-109.

[34] Tornabene, F., Brischetto, S. Fantuzzi, N. and Bacciocchi, M., 2016, Boundary Conditions in 2D Numerical and 3D Exact Models for Cylindrical Bending Analysis of Functionally Graded Structures. Shock and Vibration, 2016, pp.17.

[35] Kermani, I.D., Mirdamadi, H.R. and Ghayour, M., 2016, Nonlinear stability analysis of rotational dynamics and transversal vibrations of annular circular thin plates functionally graded in radial direction by differential quadrature. Journal of Vibration and Control, 22(10), pp.2482-2502.

[36] Abdelaziz, H.H., Amar Meziane, M.A., Bousahla, A.A., Tounsi, A., Mahmoud S.R. and Alwabli, A.S., 2017, An efficient hyperbolic shear deformation theory for bending, buckling and free vibration of FGM sandwich plates with various boundary conditions. Steel and Composite Structures, 25(6), pp.693-704.

[37] Liew, K., Yang, J. and Wu, Y., 2006, Nonlinear vibration of a coating-FGM-substrate cylindrical panel subjected to a temperature gradient. Computer Methods in Applied

Mechanics and Engineering, 195(9), pp.1007-1026.

[38] Pradhan, S. and Murmu, T., 2009, Thermo-mechanical vibration of FGM sandwich beam under variable elastic foundations using differential quadrature method. Journal of Sound and Vibration, 321(1), pp.342-362.

[39] Lu, C.F. and Chen, W., 2005, Free vibration of orthotropic functionally graded beams with various end conditions. Structural Engineering and Mechanics, 20(4), pp.465-476.

[40] Vahdati, A., Salehi, M., Vahabi, M., Jafari Fesharaki, J. and Ghassemi, A., 2019, Fracture analysis of piezoelectromagnetic medium with axisymmetric cracks. Theoretical and Applied Fracture Mechanics, 104, pp.102337.

[41] Bellifa, H., Bakora A., Tounsi, A., Bousahla, A.A. and Mahmoud, S.R., 2017, An efficient and simple four variable refined plate theory for buckling analysis of functionally graded plates. Steel and Composite Structures, 25(3), pp.257-270.

[42] Yang, J., Liew, K.M., Wu, Y.F. and Kitipornchai, S., 2006, Thermo-mechanical post-buckling of FGM cylindrical panels with temperature-dependent properties. International Journal of Solids and Structures, 43(2), pp.307-324.

[43] Yas, M. and Aragh, B.S., 2011, Elasticity solution for free vibration analysis of four-parameter functionally graded fiber orientation cylindrical panels using differential quadrature method. European Journal of Mechanics-A/Solids, 30(5), pp.631-638.

[44] Bert, C. and Malik, M., 1996, Free vibration analysis of thin cylindrical shells by the differential quadrature method. Journal of pressure vessel technology, 118(1), pp.1-12.

[45] Horgan, C.O. and Chan, A.M., 1999, The Pressurized Hollow Cylinder or Disk Problem for Functionally Graded Isotropic Linearly Elastic Materials. Journal of Elasticity, 55(1), pp.43-59.

[46] Heinbockel, J.H., 2001, introduction to tensor calculus and continuum mechanics. Trafford.